4
Empirical measures of proximal and distal magnetic fields

C.A. Foss

ABSTRACT

At great distance from a magnetisation the information carried about it in the magnetic field is condensed to six parameters: the three coordinates of its centre, and the strength and orientation of its moment (the three-dimensional orientation of magnetic moment is specified by two angles). Further recession from the magnetisation does not cause loss of this information provided the field can still be detected and analysed. This is a distal field. Fields closer to the magnetisation that carry additional information about its distribution are to some degree proximal. There is a penalty that comes with the additional information in a proximal field: that it complicates and degrades recovery of information about its centre and direction of magnetisation that are (at least in theory) well conveyed by the distal field. This degradation is primarily the consequence of domination of the closest samples of the magnetic field by the closest zones of the magnetisation. It is important in magnetic field analysis and interpretation to understand the capabilities and limitations in recovering information from magnetic fields. The attempts I present in this chapter to quantify this gradual and continuous transition between distal and proximal fields are of limited success but hopefully provide insights to data-related capabilities and limitations in magnetic field analysis.

4.1 INTRODUCTION

A magnetic field is proximal to a magnetisation if it carries significant detailed information of its spatial distribution. If the only spatial information is the location of the centre of magnetisation then the magnetic field measurements are fully summarised by a dipole model and the field is completely distal. For distal magnetic fields the only two challenges in estimation of source magnetisation direction are correct isolation of the field due to that magnetisation and correct determination of the centre location of the magnetisation. As a proxy of transition between proximal and distal fields I compare misfits of dipole model fields with fields of simple alternative models rather than (as is usually done) with input measured fields. These misfits increase with proximity to the magnetisation and are dependent on the complexity of its distribution. For inversion of alternative models I assign complexity to the model bodies in three classes: (i) approximately equidimensional complexity, (ii) horizontal elongation and (iii) plunge.

To investigate inadequacy of dipole magnetisation models for a selected task I propose two analyses. The first is analysis of difference between the best-fit dipole model and the best-fit model of two independent vertically and horizontally polarised dipoles (I call this VHPD or 'vertically and horizontally polarised dipole' analysis).

The second is analysis of differences between the best-fit dipole and best-fit ellipsoid models (I call this DE or 'dipole-ellipsoid' analysis).

4.2 DIPOLES AND DISTAL AND PROXIMAL MAGNETIC FIELDS

There is continuous and gradual transition between proximal and distal fields and the degree to which a magnetic field is distal or proximal to its source depends not just on position of the source magnetisation relative to the field measurements but also on the spatial distribution of magnetisation and the spacing, precision and nature of the field measurements (e.g. total field, component, single gradient or tensor gradients). For highly proximal magnetic fields measured by low elevation or ground surface surveys over shallow subsurface magnetisations, discontinuities in the top surface of the magnetisation or near-top-of-magnetisation inhomogeneities cause sharp and high-amplitude field variations within the closest field measurements. Those local field variations are unlikely to be sufficiently sampled and their extreme amplitude variations disproportionately influence inversion, reducing confidence in the resulting models. At greater distances from the magnetisation these details of shape become much less significant and more reliable estimates of the total magnetisation can be obtained.

Descriptions of a magnetic field as proximal or distal (and the corresponding descriptions of magnetisation as 'compact' or 'distributed') specifically imply the level of information about the source magnetisation that can be recovered from a magnetic field. If a measured magnetic field can be broken into several discrete or only partially overlapping data regions within which the field is acceptably matched by dipole sources, then the field is purely distal and a list of the dipole statistics contains all of the information that can be recovered from it (note that for an ideal dipole the magnetic field becomes distal immediately external to it). A dipole magnetisation does not specify an intensity of magnetisation or a volume, only their product: the magnetic moment. Exactly the same dipole magnetic field variation due to a homogeneously magnetised sphere is generated by any co-centred sphere with the same magnetic moment and with purely radial variation in intensity and/or direction of magnetisation (i.e. consisting of shells of homogeneous magnetisation). Dipole source models leave some information unrecovered from the magnetic fields of irregular and complex (distributed) magnetisations.

The most pertinent question on first examining an image of a magnetic field is how distal or proximal various parts of the field are to their source magnetisations. This question is the starting point to evaluate how much information can be recovered from the magnetic field data and to develop strategies by which to achieve it. Note that meaningful evaluation of a magnetic field requires knowledge of the distribution of its individual measurement locations to appreciate how the level of detail in the field may be influenced by the density at which it is sampled. It is especially important to know the distribution of measurements before interpreting or inverting magnetic field grids because grid data is often separated from the primary measurements from which it was generated.

4.3 VERTICALLY AND HORIZONTALLY POLARISED DIPOLE (VHPD) AND DIPOLE-ELLIPSOID (DE) ANALYSES

We can attempt to match a magnetic anomaly that might be due to a dipole magnetisation with two dipoles of independent location and strength, one of a vertically directed magnetisation and the other with a magnetisation in the horizontal plane. If the anomaly is indeed due to a dipole source and has been correctly separated from other field variations then inversion should co-locate the two polarised dipoles, the vector sum of their magnetisations is the true dipole magnetisation, and the field is distal. If the dipoles are not co-centred or if there is a significant coherent residual misfit to the input field then the magnetisation is not completely dipolar and the field measurements are to some degree proximal to the magnetisation.

A second, separate dipole-ellipsoid (DE) test of inadequacy of a dipole model is the change in magnetisation parameters on replacing the best-fit dipole model with a more complex best-fit ellipsoid model. This test has the advantage that an ellipsoid is a physically meaningful model (which separated VHPD sources are not) and that ellipsoids supply what may prove significant additional parameter values and upgrades of dipole-based parameter estimates. VHPD and DE model analyses provide related but different measures of inadequacy of dipole models that may be able to contribute towards evaluation of a magnetic field as predominantly distal or predominantly proximal.

4.4 VHPD DECOMPOSITION OF A SYNTHETIC DATA DIPOLE ANOMALY

Figure 4.1 illustrates VHPD analysis of an input field from a dipole source. The input field (Fig. 4.1A) is due to a homogeneous sphere of radius 100 m, depth 200 m and magnetisation 2 Amp/metres with declination 135° and inclination +45°. The geomagnetic field setting of this model has a strength of 60,000 nT, declination 0° and inclination −60°. TMI is computed at 25 m intervals across a square array of 800 m side length centred on the source magnetisation. Figure 4.1B shows TMI computed from the pre-inversion polarised dipoles starting model. Both starting polarised dipoles have magnetisations of 1 A/m and the horizontal magnetisation has a declination of 80°. The bodies are displaced by 16 and 243 m from the source solution. The inversion model has nine free parameters – the X, Y and Z coordinates of the two bodies, the intensity of magnetisation of the bodies and the declination of magnetisation of the horizontally magnetised body. Despite the substantial misfit of the starting model this inversion successfully and rapidly converges to an almost perfect fit to the input field. The final body locations are coincident with the primary model to within 1 m both horizontally and vertically and the vector sum of their magnetisations agrees within 1° with the primary model. The individual fields of the final inversion polarised dipoles are shown in Fig. 4.1C and 4.1D. It is the summation of these fields that matches the input field shown in Fig. 4.1A. All other test inversions with input dipole model data have produced similarly successful results.

The purpose of VHPD analysis is to provide a model-based rather than a data-based measure of the insufficiency of a dipolar model and thereby indicate the degree of transition between a distal field and a proximal field. Several statistics can be derived from imperfection of a VHPD analysis as presented in the following synthetic data and measured case study inversions. The four statistics computed from VHPD analysis presented below each have a corresponding statistic in D-E analysis.

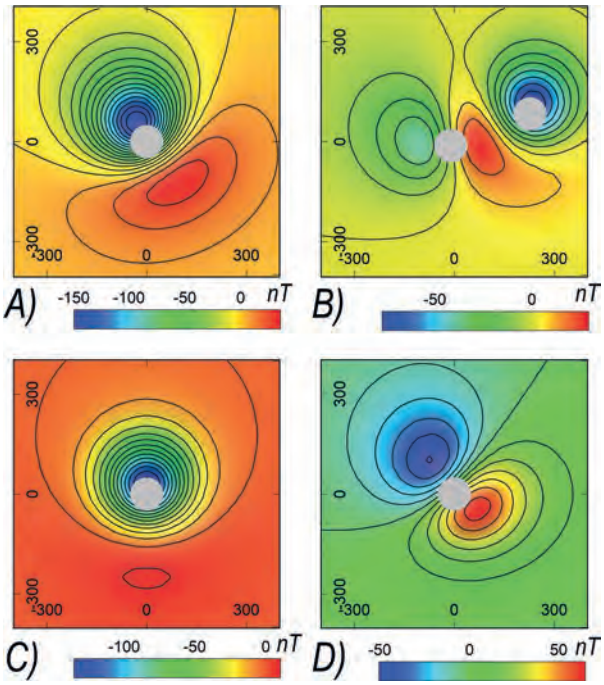

Fig. 4.1. A) TMI due to a dipole magnetisation of declination 135°, inclination +45°, B) inversion starting model TMI, C) TMI of the vertically polarised dipole and D) TMI of the horizontally polarised dipole.

4.5 DIPOLE MODEL DEPARTURE STATISTICS

I present four statistics to indicate departure of a VHPD model and an ellipsoid model from that of a dipole model recovered from inversions of the same data. Parameters of the dipole, VHPD and ellipsoid models are listed in Table 4.1 followed by derivation of statistics quantifying differences between VHPD and dipole models and between ellipsoid and dipole models.

Table 4.1. Model parameter terminology.

Model	Magnetic moment	Intensity	Declination	Inclination	Centre E	Centre N	Centre Z	Radius	Volume
Best-fit dipole	$\mathbf{M}_d$	Int_d	Dec_d	$Inc._d$	X_d	Y_d	Z_d	r_d	vol_d
Vertically polarised dipole	$\mathbf{M}_{VPD}$	Int_{vp}	0	+/−90	X_{vp}	Y_{vp}	Z_{vp}	r_d	vol_d
Horizontally polarised dipole	$\mathbf{M}_{HPD}$	Int_{hp}	Dec_{VHPD}	0	X_{hp}	Y_{hp}	Z_{hp}	r_d	vol_d
Best-fit ellipsoid	$\mathbf{M}_e$	Int_e	Dec_e	$Inc._e$	X_e	Y_e	Z_e	r_e*	vol_e
VHPD pair	$\mathbf{M}_{VHPD}$	Int_{VHPD}	Dec_{VHPD}	$Inc._{VHPD}$	X_{VHPD}	Y_{VHPD}	Z_{VHPD}	r_d	vol_d

* $r_e = (ra \times rb \times rc)^{1/3}$ where ra, rb, rc are the ellipsoid radii

The VHPD model of a pair of dipoles of identical volume, one with vertically and one with horizontally polarised magnetisation has the following effective magnetisation direction and centre of magnetisation for a field at a large distance compared to the dipole separation:

$$\text{Intensity of magnetisation: } Int_{VHPD} = \sqrt{(Int_{vp}^2 + Int_{hp}^2)}$$

$$\text{Inclination of magnetisation: } Inc_{VHPD} = \text{asin}(Mz_{VHPD}, Mh_{VHPD})$$

$$\text{East centre of magnetisation: } X_{VHPD} = X_{vp} + (X_{hp}-X_{vp})* Int_{hp}/(Int_{vp} + Int_{hp})$$

$$\text{North centre of magnetisation: } Y_{VHPD} = Y_{vp} + (Y_{hp}-Y_{vp})* Int_{hp}/(Int_{vp} + Int_{hp})$$

$$\text{Depth to centre of magnetisation: } Z_{VHPD} = Z_{vp} + (Z_{hp}-Z_{vp})* Int_{hp}/(Int_{vp} + Int_{hp})$$

$$\text{Direction of magnetisation: } (Dec_d, Inc._d)$$

The following analysis statistics describe differences between dipole and VHPD models and between dipole and ellipsoid models. They are designed to highlight differences between a dipole inversion model and VHPD or ellipsoid inversion models that arise from permitting additional degrees of freedom in the inversions.

4.5.1 Statistic 1 – angular separations between pairs of model magnetisation directions

S1_VHPD (measured in degrees) is the angular separation between the VHPD and dipole model magnetisation directions:

$$(Dec_{VHPD}, Inc._{VHPD}) - (Dec_d, Inc._d)$$

S1_DE (measured in degrees) is the angular separation between the dipole and ellipsoid model magnetisation directions:

$$(Dec_e, Inc._e) - (Dec_d, Inc._d)$$

4.5.2 Statistic 2 – magnitude of the magnetisation difference between pairs of models

VHPD_2: magnitude of the vector difference between the VHPD magnetisation and the dipole model magnetisation normalised to the dipole model intensity and converted to a percentage:

$$S2\_VHPD = 100 * \left|M_{VHPD} - M_d\right| / Int_d$$

S2_DE: magnitude of the vector difference between the dipole and ellipsoid total magnetisations normalised to the dipole magnetisation and converted to a percentage:

$$S2\_DE = 100 * \left|M_d - vol_e/vol_d * M_e\right| / Int_d$$

4.5.3 Statistic 3 – horizontal separation between model magnetisation centres

S3_VHPD: summed horizontal separations of the VHPD magnetisations from the dipole centre weighted by their relative intensities, normalised to depth and converted to a percentage:

$$S3\_VHPD = 100 * ((Int_{vp} / Int_{VHPD}) * \sqrt{((X_{vp} - X_d)^2 + (Y_{vp} - Y_d)^2)} + (Int_{hp} / Int_{VHPD}) * \sqrt{((X_{hp} - X_d)^2 + (Y_{hp} - Y_d)^2)}) / Z_d$$

S3_DE: horizontal separation of the ellipsoid magnetisation from the dipole centre normalised to depth of the dipole and converted to a percentage:

$$S3\_DE = 100 * \sqrt{((X_e - X_d)^2 + (Y_e - Y_d)^2)} / Z_d$$

4.5.4 Statistic 4 – product of statistics 1 to 3

$$S4\_VHPD = S1\_VHPD * S2\_VHPD * S3\_VHPD$$

$$S4\_DE = S1\_DE * S2\_DE * S3\_DE$$

4.6 DIPOLE-ELLIPSOID (DE) ANALYSIS

A natural geometric extension of model complexity to improve the fit to a measured field from that achieved with a dipole (hopefully thereby achieving an improved representation of the true magnetisation) is to convert a spherical magnetisation model to an ellipsoid model with three axes of variable length. Analytic solutions to compute the magnetic field of an ellipsoidal magnetisation have been derived by Clark *et al*. (1986). An ellipsoid is a very versatile form. If the three radii have similar lengths the body is little different to a sphere and shares a weak sensitivity to individual values of volume and intensity of magnetisation. If one radius is much longer than the other two (the ellipsoid has a cigar shape) there is greater sensitivity to the length of the longest axis (that

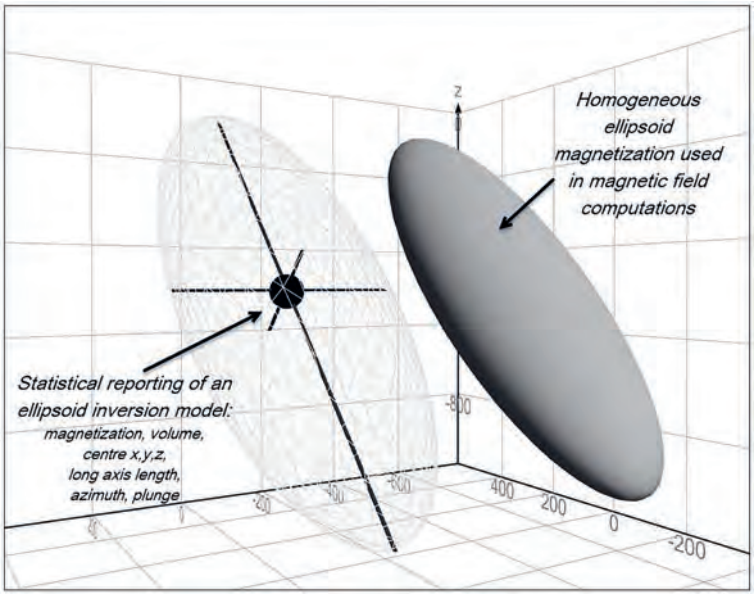

Fig. 4.2. Statistics summarising the distribution of magnetisation of an ellipsoid model.

can be oriented in any three-dimensional direction) than to the other two axes. If one radius (that again can have any three-dimensional orientation) is much shorter than the other two then the ellipsoid has a plate-like shape with reduced sensitivity to the length of the shortest radius. Note that as the shape of the ellipsoid progressively deviates from that of a sphere there are increasing issues of directional sensitivity to factors such as magnetisation direction and separation of the anomaly from the background field. Justification for increasing the complexity of the model from a sphere to an ellipsoid depends on the interpreted significance of the reduced misfit to the measured field which that achieves and the interpreted geological viability of the dipole or ellipsoid body shapes. Just as for a spherical model, an ellipsoid model should be visualised as providing statistical parameters of the distribution of magnetisation rather than the directly representing it (see Fig. 4.2). Alternative extensions of model complexity can be achieved with a variety of shapes using faceted bodies.

4.7 VHPD AND DE ANALYSIS OF COMPLEX EQUIDIMENSIONAL MAGNETISATION

Figure 4.3 shows images of TMI at elevations 50 and 200 m above a complex equidimensional magnetisation of ~300 m side length. At the lower and upper elevations, separations between the top of magnetisation and the closest field measurements are respectively 17% and 67% of the horizontal extent of the magnetisation. It might

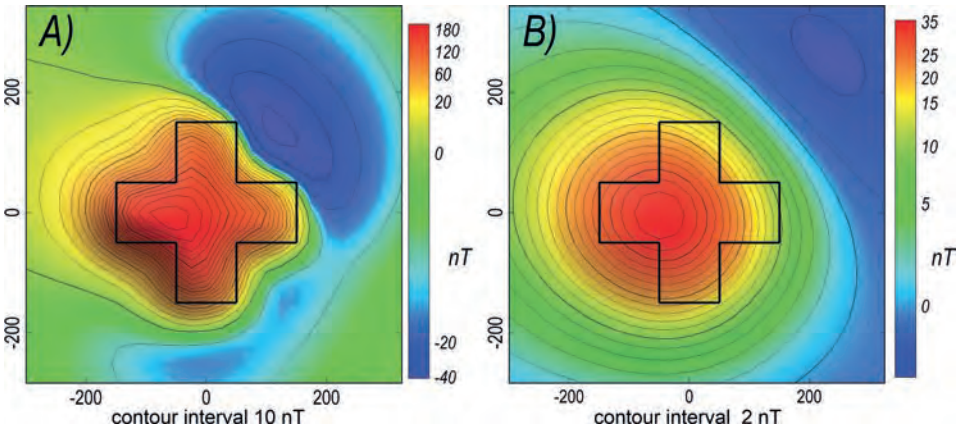

Fig. 4.3. TMI over a complex magnetisation of declination 225°, inclination −45° at elevations of A) 50 m and B) 200 m.

seem that such a directly pertinent statistic would be valuable for discriminating between distal and proximal fields, but this measure has no practical value in analysis of measured field data unless the true depth and horizontal extent of the source magnetisation are already known.

Figure 4.4 shows contours of the input model field and best-fit dipole inversion field at both elevations. At the higher elevation a dipole model clearly provides a closer fit to the field of the original model than it does at the lower elevation. At both elevations the horizontal centres of the dipoles are close to the horizontal centres of the input model and the magnetisation direction estimates provided by the dipole inversions of the fields are only different from the true magnetisation direction by 1.2° and 0.6° degrees at the lower and upper elevations respectively (see Table 4.2).

Differences in magnetisation direction and separations of the vertically and horizontally polarised

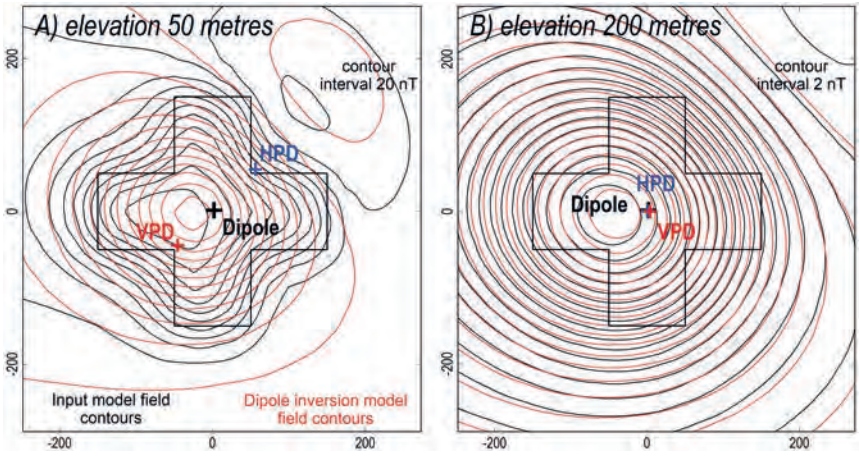

Fig. 4.4. Source (black) and dipole inversion model (red) TMI contours at A) 50 m and B) 200 m elevations above the top of magnetisation. Crosses mark the centres of the dipole and vertically and horizontally polarised dipoles.

Table 4.2. Equidimensional magnetisation study: model statistics from inversion of field data at 50 m and 200 m.

Model	Xc	Yc	Zc	J (A/m)	Vol (m^3)	Dec	Inc.	Rotation	Data misfit %
Source_50	0	0	100	1	5,000,000	225	–45	–	–
Dipole_50	1.7	1.7	178	2.016	4,188,790	225	–43.8	1.2°	27
Dip_V_50	–46	–44	178	1.234	4,188,790	000	–90	–	–
Dip_H_50	56	55	178	0.928	4,188,790	224.6	0	–	–
VHPD_50	–2.2	–1.4	178	1.552	4,188,790	224.6	–53.3	8.3°	24
Ellipsoid_50	1.1	0.7	93.7	4.450	1,090,699	225.4	–44.3	0.8°	18
Source_200	0	0	250	1	5,000,000	225	–45	–	–
Dipole_200	1.5	0.6	290	1.394	4,188,790	225.5	–44.4	0.6°	5
Dip_V_200	3.8	0.2	290	0.977	4,188,790	000	–90	–	–
Dip_H_200	0.3	0.7	290	1.006	4,188,790	224.8	0	–	–
VHPD_200	2.0	0.5	290	1.403	4,188,790	224.8	–44.2	0.8°	5
Ellipsoid_200	0.5	0.4	247.8	1.347	3,694,336	225	–44.9	0.1°	1

Differences of the VHPD analysis and ellipsoid model from the dipole model

Model	Statistic1	Statistic2	Statistic3	Statistic4	% Data misfit
VHDP_50	9°	27	3	729	13
VHDP_200	0.6°	1	0.2	0.12	1
ellipsoid_50	0.6°	43	0.7	18	21
ellipsoid_200	0.6°	15	0.4	3.6	5

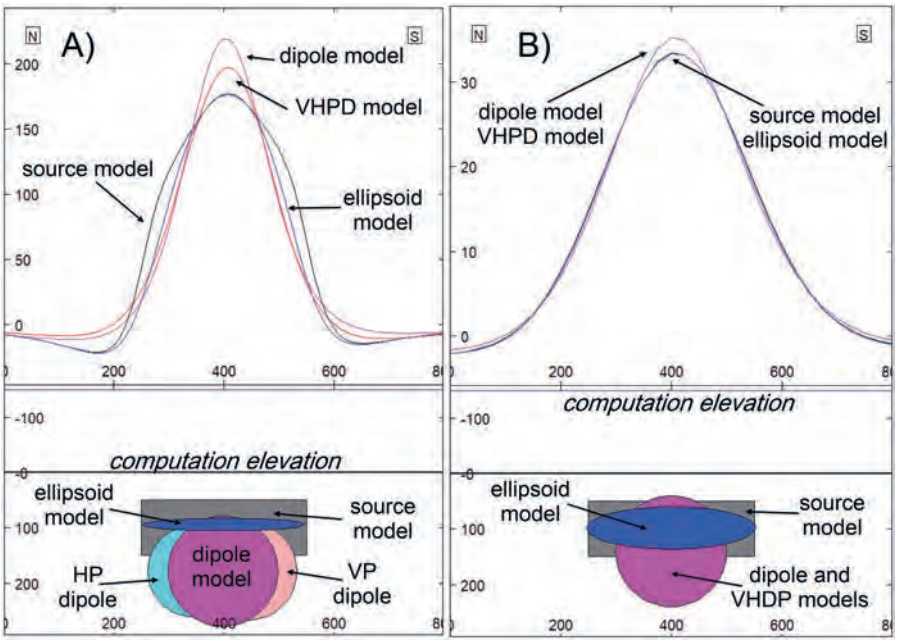

Fig. 4.5. Central north to south profiles at elevations of A) 50 m and B) 200 m above the top of the source model.

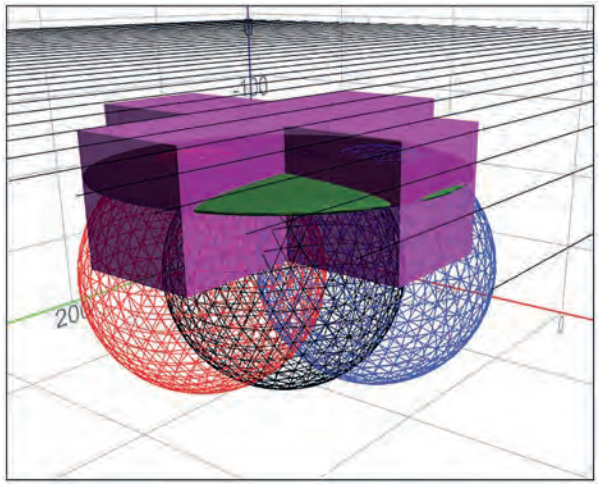

Fig. 4.6. Perspective of the source model (magenta), ellipsoid (green) and dipole (black mesh) models, and the vertically (red mesh) and horizontally (blue mesh) polarised VHPD bodies from inversions of the field at 50 m elevation.

dipoles for analyses at the lower and upper elevations show clear differences between more proximal and more distal fields. A central north–south section through the models and the computed fields at the two elevations is shown in Fig. 4.5. For inversions of the lower elevation data (Fig. 4.5A) the input model field is poorly matched by the single dipole and VHPD inversions. It is, however, more closely matched by the ellipsoid inversion model that is almost co-centred with the input model. For inversions of the higher elevation data (Fig. 4.5B) the data misfits are all substantially reduced and the single dipole and the polarised dipoles are coincident and almost co-centred with the input model. A perspective view of the lower elevation inversion models is shown in Fig. 4.6. Because the input model has two axes of horizontal symmetry there is little shape bias to produce a significant horizontal displacement of the dipole or ellipsoid inversion models. In keeping with strong linkage between estimation of the horizontal location of a magnetisation and of its direction, lack of substantial horizontal displacement of these bodies is matched by small differences of their magnetisation directions from that of the input model.

4.8 VHPD AND DE ANALYSIS OF HORIZONTALLY ELONGATE MAGNETISATION

The previous study investigated analysis of fields due to a complex but equidimensional distribution of magnetisation. If a magnetisation is elongated along a horizontal axis there is reduced sensitivity in recovery of both its spatial and magnetisation properties. Figure 4.7 shows magnetic fields computed at an elevation 50 m above a homogeneous-magnetisation, elliptic-section pipe with horizontal top and base surfaces, a north-east–south-west long axis of 300 m length and a short axis of 100 m.

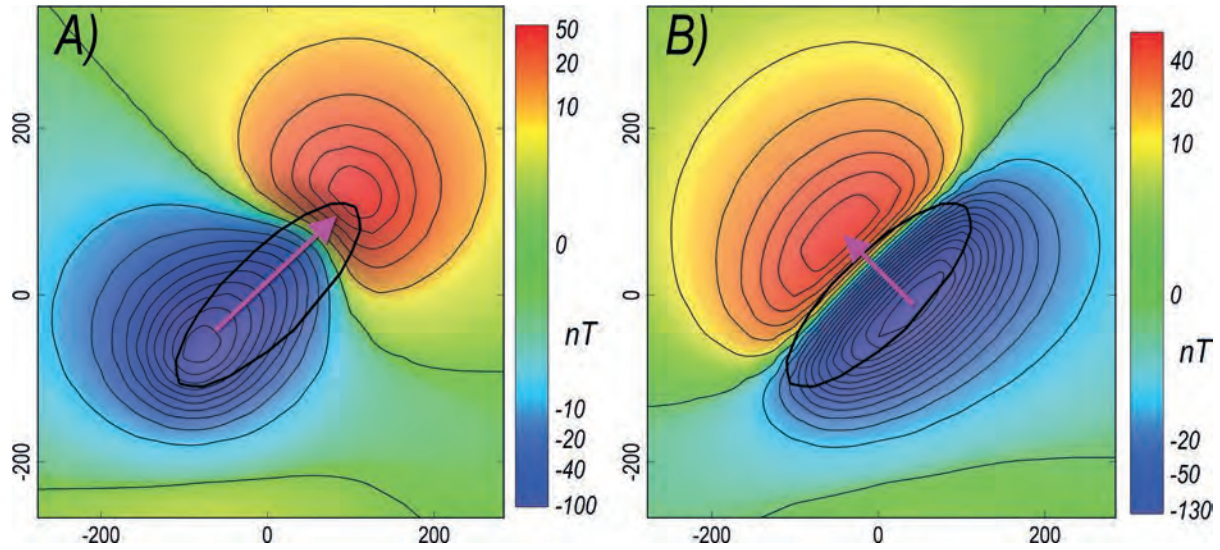

Fig. 4.7. TMI computed at an elevation of 50 m above a SW–NE trending elliptic pipe of axis lengths 150 and 50 m. Magnetisations: A) axial declination of 45° inclination +15°, B) transverse declination of 315° inclination +15°.

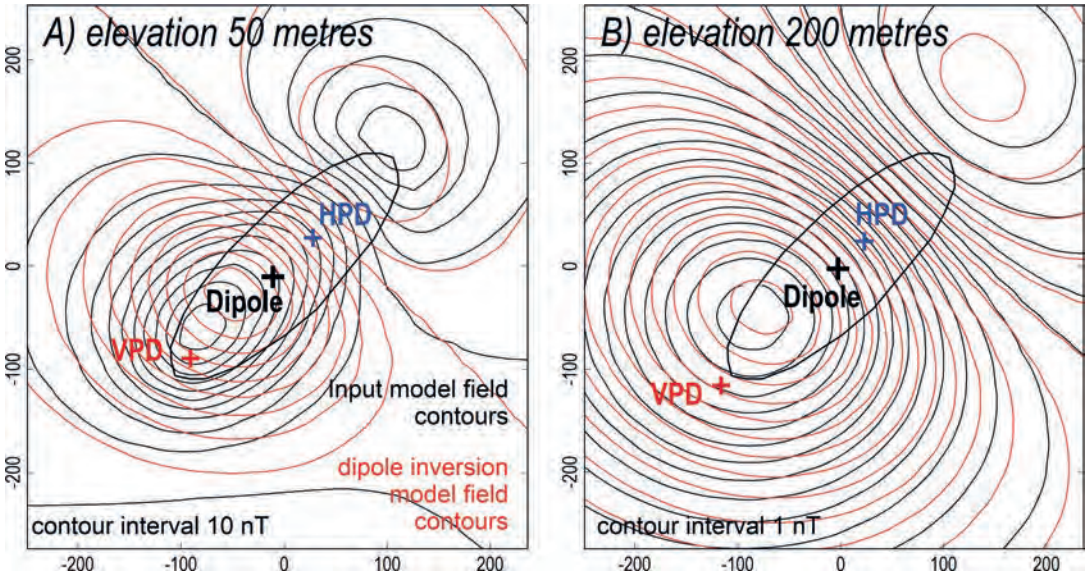

Fig. 4.8. TMI contours of the input model with a long-axis (045°) magnetisation (black) and dipole inversion model (red) at A) 50 m elevation and B) 200 m elevation.

In Fig. 4.7A the magnetisation is parallel to the long axis and in Fig. 4.7B it is parallel to the short axis. The ratios of the separation distance between the closest magnetisation and magnetic field computation at the two investigated elevations of 50 and 200 m to the long axis of magnetisation are 1:6 and 1:1.5 respectively. At the relatively steep geomagnetic inclination, regardless of body shape and orientation the TMI anomaly trough-to-peak azimuths approximately indicate the declination of magnetisation.

Figure 4.8 shows TMI contours (in black) for the input model field with magnetisation parallel to the long axis and (in red) for the dipole inversion model. The field at 50 m elevation is shown in Fig. 4.8A and the field at 200 m elevation is shown in Fig. 4.8B. The contour match is clearly closer at the higher elevation at which there is less influence of body shape. For the VHPPD analysis of this elongate source body there is significant separation of the two polarised dipoles at both elevations. Despite this, the error in estimated magnetisation direction of

Table 4.3. Elongate magnetisation study: model statistics from inversion of field data at 50 m and 200 m above the input model 'Source-50' with magnetisation parallel to elongation.

Model	Xc	Yc	Zc	J (A/m)	Vol (m^3)	Dec	Inc.	Rotation	Misfit %
Source_50	0	0	100	1	2,344,250	045	+15	–	–
Dipole_50	–11	–10.2	167	0.848	4,188,790	044.1	23	8 °	34
Dip_V_50	–91	–90	167	0.323	4,188,790	000	90	–	–
Dip_H_50	28	28	167	0.584	4,188,790	044.3	0	–	–
VHPD_50	–14	–14	167	0.667	4,188,790	044.3	29	14°	27
Ellipsoid_50	0.3	0.2	82	0.792	2,634,354	045.0	14.6	0.4°	5
Source_200	0	0	250	1	2,344,250	045	+15	–	–
Dipole_200	–2.8	–2.3	285	0.642	4,188,790	044.8	16.2	1.2°	8
Dip_V_200	–116	–116	285	0.165	4,188,790	000	90	–	–
Dip_H_200	26	27	285	0.488	4,188,790	045	0	–	–
VHPD_200	–10	–9	285	0.515	4,188,790	045	18.7	4°	7
Ellipsoid_200	0.2	0.1	245	0.388	3,694,336	045	15.0	0°	0.4

Differences of the VHPD analysis and ellipsoid model from the dipole model

Model	Statistic1	Statistic2	Statistic3	Statistic4	% Data misfit
VHDP_50	6°	23	3	414	20
VHDP_200	2.5°	20	3	150	7
ellipsoid_50	8°	43	9	3,096	36
ellipsoid_200	1.2°	47	1.3	73	8

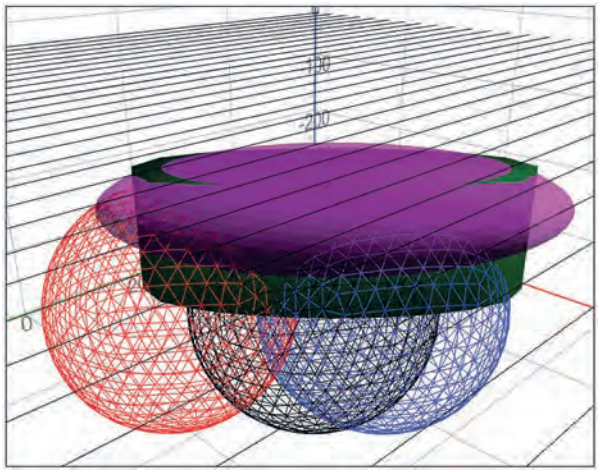

Fig. 4.9. Perspective of the source (green), ellipsoid (magenta), dipole (black mesh), vertical (red mesh) and horizontal (blue mesh) polarised VHPD bodies from inversions of the field computed at 200 m above the source model.

the VHPD model is reduced from 14° in the lower elevation field to 4° in the higher elevation field as reported in Table 4.3. Errors in magnetisation direction of the dipole model at the two elevations are 8° and 1.2° respectively. Figure 4.9 shows a perspective view of all the models from inversion of the 200 m elevation data. Both the dipole and ellipsoid inversion models are horizontally co-centred with the input model but the additional shape complexity of the ellipsoid gives it the freedom to more closely match the field of the input model. The errors in magnetisation direction of the ellipsoid inversion model are only 0.4° at 50 m elevation and less than 0.1° at 200 m elevation (see Table 4.3).

Figure 4.10 shows (in black) TMI contours of the field computed from the input model with magnetisation parallel to the short axis, and (in red) TMI contours of the field computed from the dipole inversion. Figure 4.10A is at 50 m elevation and Fig. 4.10B is at 200 m elevation. Misfit between the two model fields reduces significantly from the lower elevation to the higher elevation. Model statistics are listed in Table 4.4. The statistics designed to indicate whether a field is more distal or more proximal show less variation with elevation for magnetisation parallel to the short axis of the body (Table 4.4) than for magnetisation parallel to body elongation (Table 4.3) revealing that alignment of magnetisation with the direction of elongation of the body accentuates the magnetic field expression of body shape.

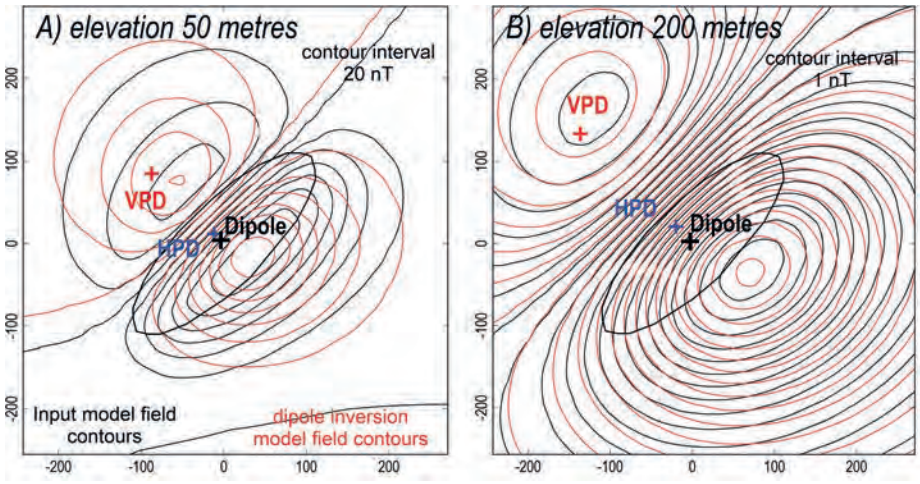

Fig. 4.10. TMI contours of the elliptic-pipe model with a short-axis (315°) magnetisation (black) and dipole inversion model (red) at A) 50 m elevation and B) 200 m elevation.

Table 4.4. Elongate magnetisation study: model statistics from inversion of field data at 50 m and 200 m above the input model 'Source-50' with magnetisation perpendicular to elongation.

Model	Xc	Yc	Zc	J (A/m)	Vol (m^3)	Dec	Inc.	Rotation	Misfit %
Source_50	0	0	100	1	2,344,250	315	+15	–	–
Dipole_50	–4	4	124	0.696	4,188,790	314.2	9.7	5°	30
Dip_V_50	–88	85	124	0.143	4,188,790	000	90	–	–
Dip_H_50	–12	12	124	0.825	4,188,790	314.3	0	–	–
VHPD_50	–23	23	124	.849	4,188,790	314.3	9.7	5°	28
Ellipsoid_50	0.2	–0.7	88	.602	3,554,152	315.1	15.4	0.4°	3
Source_200	0	0	250	1	2,344,250	315	+15	–	–
Dipole_200	–3	3	263	0.596	4,188,790	314.8	13.4	1.6°	7
Dip_V_200	–114	111	263	0.129	4,188,790	000	90	–	–
Dip_H_200	–17	17	263	0.653	4,188,790	314.7	0	–	–
VHPD_200	–33	32.5	263	0.666	4,188,790	314.7	11.2	5°	7
Ellipsoid_200	0.2	–0.2	248	1.424	1,634,620	315.0	15	0°	0.3

Differences of the VHPD analysis and ellipsoid model from the dipole model

Model	Statistic1	Statistic2	Statistic3	Statistic4	% Data misfit
VHDP_50	3.7°	20	22	1,628	31
VHDP_200	2.2°	12	16	422	11
ellipsoid_50	5.8°	28	5.1	828	12
ellipsoid_200	1.6°	7	1.7	19	8

4.9 SYNTHETIC-DATA VHPD AND DE ANALYSIS OF A PLUNGING MAGNETISATION

A key trade-off between spatial and magnetisation parameters in finding a magnetisation to explain a measured magnetic field variation is between the spatial plunge of the magnetisation and the inclination of its magnetisation. For semi-infinite thin sheets of magnetisation this trade-off is extreme with the two angles combining into a single term (Hood 1964). For more horizontally compact sources, such as pipes, the trade-off is less effective. However, even for a pipe of circular section an error in either angle can substantially compensate for a corresponding error in the other. This leads to collaborative reduction of sensitivity in

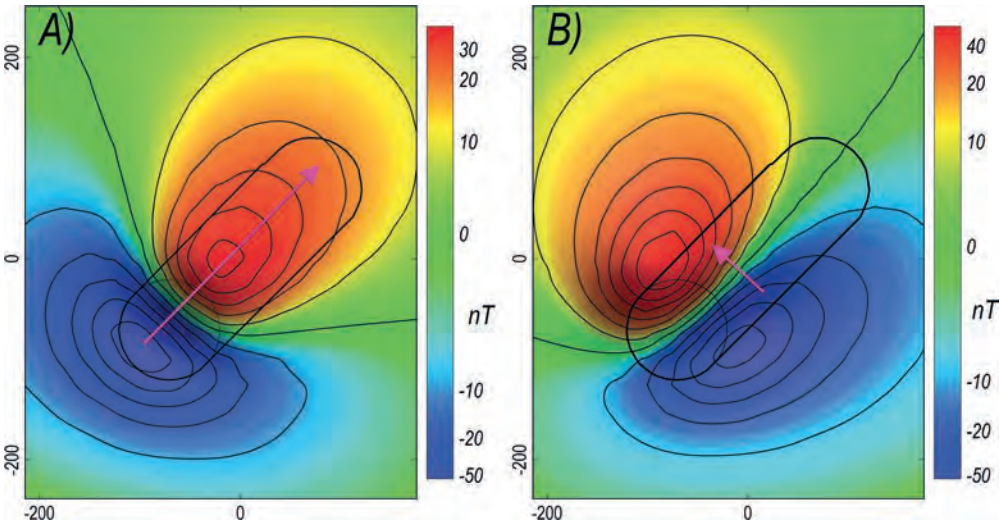

Fig. 4.11. TMI images at 50 m elevation over circular pipes plunging to the north-east with A) an axial declination of 45°and B) a transverse declination of 315°.

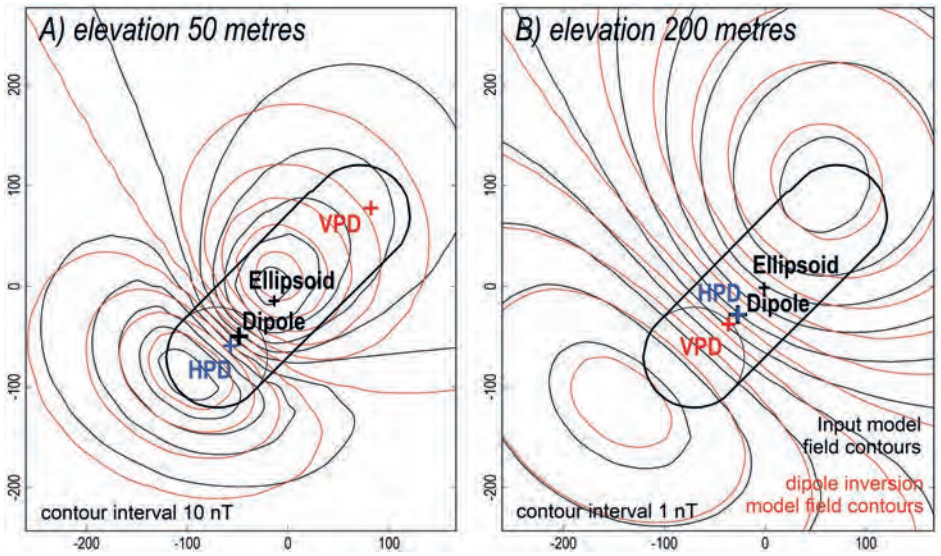

Fig. 4.12. TMI contours of the input model with a down-dip declination (45°) magnetisation (black) and dipole inversion model (red) at A) 50 m elevation and B) 200 m elevation.

estimation of both the inclination of magnetisation and spatial plunge. Figure 4.11 shows TMI images at an elevation of 50 m over a circular pipe plunging at 45° to the north-east with a declination of magnetisation in the down-plunge direction (Fig. 4.11A) and a declination of magnetisation in the north-west strike direction (Fig. 4.11B). In both cases the declination of magnetisation is reliably indicated by the trough to peak azimuth of the TMI anomalies. Figure 4.12 shows TMI contours for the input models (in black) and the single dipole inversion models (in red) for inversions of the lower, more proximal field data (Fig. 4.12A) and for inversion of the higher, more distal field data (Fig. 4.12B). The single-dipole model from inversion of the more proximal data is displaced from the centre of the input model in the up-dip direction because of the higher weighting of that shallow section of magnetisation. The single-dipole model from inversion of the more distal field is closer to the centre of the input model because the differential weighting of the top of the magnetisation is reduced (for a truly distal field the shape influence attenuates completely and the apparent centre of magnetisation is at its true position). For the VHPD model there is a substantial horizontal displacement between the vertically and horizontally polarised

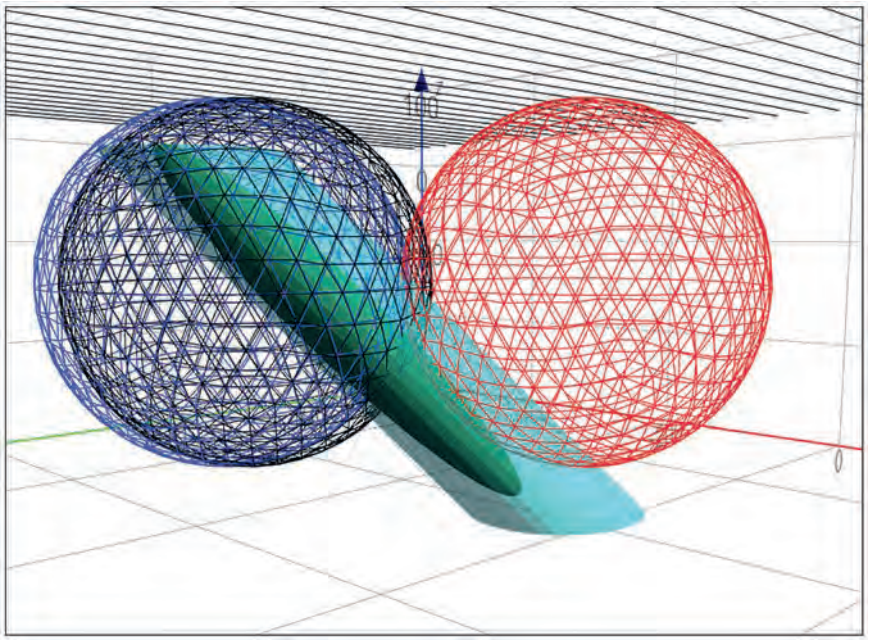

Fig. 4.13. Perspective of the plunging pipe source (solid light blue), ellipsoid (solid green) and dipole (black mesh) models, and the vertical (red mesh) and horizontal (blue mesh) polarised VHPD bodies from inversions of the field 50 m above the top of the source model.

dipoles in the lower, more proximal field (Fig. 4.12A) with reduced displacement in the more distal 200 m elevation field (Fig. 4.12B).

Figure 4.13 is a perspective view of the input and inversion models for the field at 50 m elevation. The ellipsoid inversion develops a cigar shape to match the input pipe model and the two bodies are approximately co-centred. The dipole model, however, cannot match the input model shape and is centred towards the top of the pipe model.

Figure 4.14 shows TMI contours for the input models (black) and the dipole inversion models (red) for magnetisations with declination in the along-strike direction at the lower 50 m elevation (Fig. 4.14A) and at the higher 200 m elevation (Fig. 4.14B). Just as for the horizontally elongate bodies, magnetisation in the transverse direction reduces the influence of distribution shape. This has a significant influence on characterisation of the field as being more proximal or more distal.

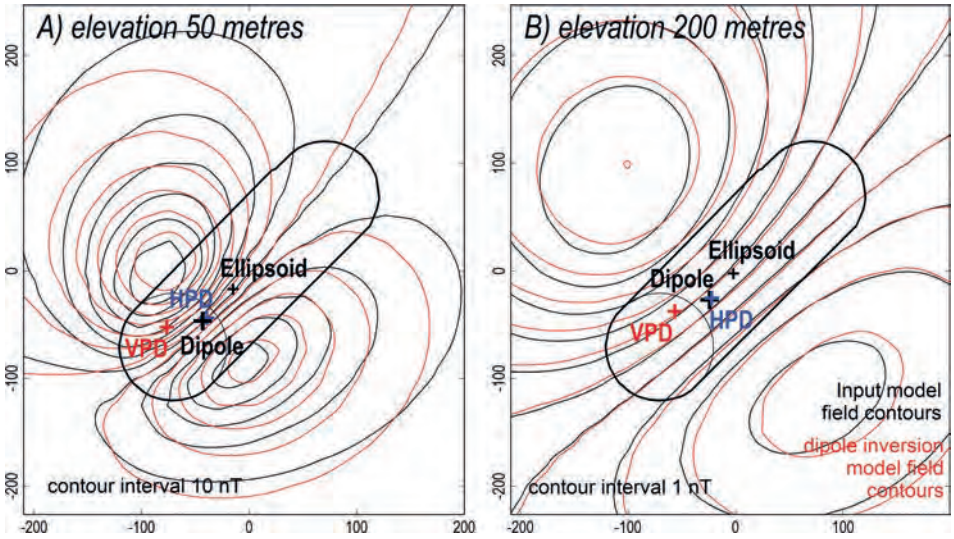

Fig. 4.14. TMI contours of the input model with an along-strike (declination 315°) magnetisation (black) and dipole inversion model (red) at A) 50 m elevation and B) 200 m elevation.

4.10 PERFORMANCE OF THE PROXIMAL/ DISTAL STATISTICS

As shown by these inversion studies, many factors influence the magnetic field expression of a magnetisation and therefore the transition between proximal and distal fields. The studies presented of complex but equidimensional magnetisations (Figs 4.3 to 4.6 and Table 4.2), magnetisations with elongation along a single horizontal axis (Figs 4.7 to 4.10 and Tables 4.3 and 4.4) and plunging magnetisations (Figs 4.11 to 4.14 and Tables 4.5 and 4.6) show that it is simplistic to consider that any single statistic can summarise the proximal/ distal nature of a set of magnetic field measurements to a distribution of magnetisation. However, with the range of proposed statistics in Section 4.5 I attempt to approximately discriminate the degree to which a field is proximal or distal to its source magnetisation without prior knowledge of that magnetisation. Figure 4.15 plots values of statistics S1, S2 and S3 for VHPD and D-E analysis. The circle and cross symbols show the various statistics for more proximal and more distal fields respectively, as computed for the various classifications of magnetisation shape (columns A to E in Figs 4.15 and 4.16). The left side of Fig. 4.15 shows results from the VHPD analyses and the right side shows results of the DE analyses. Individual statistics behave differently between the classes of magnetisation distribution. This suggests that combination of statistics may provide better discrimination of distal and proximal fields than any individual statistic. Figure 4.16 similarly summarises the compound statistic 4 (given by the product of statistics 1 to 3) together with inversion data misfit statistics. What is required of the statistics plotted in Figs 4.15 and 4.16 to discriminate between distal and proximal fields is a reliable separation between their values in distal and proximal fields (the cross and circle symbols) and ideally a consistent separation for each class of magnetisation distribution. In Fig. 4.15 the model misfit statistics mostly (but not consistently) have higher values in the more proximal field. The data misfit statistics and compounded model misfit statistics (S4) plotted in Fig. 4.16 are more consistent indicators of proximal or distal fields but are still not reliable in all cases.

Table 4.5. Plunging magnetisation study: model statistics from inversion of field data at 50 m and 200 m above the input model 'Source-50' with magnetisation in the down-dip (45°) direction.

Model	Xc	Yc	Zc	J (A/m)	Vol (m^3)	Dec	Inc.	Rotation	Misfit %
Source_50	0	0	150	1	1,552,914	045	–15	–	–
Dipole_50	–49	–50	122	0.287	4,188,790	044.5	–9.0	6°	23
Dip_V_50	82	78	122	0.0353	4,188,790	000.0	–90	–	–
Dip_H_50	–57	–59	122	0.272	4,188,790	044.6	0	–	–
VHPD_50	–41	–43	122	.274	4,188,790	44.6	–7.3	8°	22
Ellipsoid_50	–14	–15	143	3.461	435,597	044.9	–14.6	0.4°	8
Source_200	0	0	300	1	1,552,914	045	–15	–	–
Dipole_200	–27	–28	292	0.361	4,188,790	044.7	–13.0	2°	8
Dip_V_200	–36	–38	292	.0814	4,188,790	000.0	–90	–	–
Dip_H_200	–27	–28	292	.360	4,188,790	044.8	0	–	–
VHPD_200	–29	–30	292	.369	4,188,790	044.8	–13	2°	8
Ellipsoid_200	–1	–2	302	13.84	116,831	045.0	–15.0	0°	0.9

Differences of the VHPD analysis and ellipsoid model from the dipole model

Model	Statistic1	Statistic2	Statistic3	Statistic4	% Data misfit
VHDP_50	1.6°	5	9	72	18
VHDP_200	2.0°	2	1	4	1
ellipsoid_50	5.6°	27	41	6,199	23
ellipsoid_200	2.0°	8	13	208	8

Table 4.6. Plunging magnetisation study: model statistics from inversion of field data 50 m and 200 m above the top of the input model with magnetisation in the strike (315°) direction.

Model	Xc	Yc	Zc	J (A/m)	Vol (m^3)	Dec	Inc.	Rotation	Misfit %
Source_50	0	0	150	1	1,552,914	315	–15	–	–
Dipole_50	–43	–47	115	.285	4,188,790	316.3	–12.6	3°	16
Dip_V_50	–77	–52	115	0.0685	4,188,790	0	–90	–	–
Dip_H_50	–39	–44	115	0.259	4,188,790	323.1	0	–	–
VHPD_50	–47	–46	115	0.268	4,188,790	323.1	–14.9	8°	15
Ellipsoid_50	–15	–17	129	0.197	6,982,113	315.0	–14.5	0.5°	6
Source_200	0	0	300	1	1,552,914	315	–15	–	–
Dipole_200	–24	–27	281	0.341	4,188,790	315.5	–14.2	0.9°	5
Dip_V_200	–57	–38	281	0.085	4,188,790	0	–90	–	–
Dip_H_200	–22	–25	281	0.322	4,188,790	319	0	–	–
VHPD_200	–29	–28	281	0.333	4,188,790	319	–14.8	4°	5
Ellipsoid_200	–2.1	–2.5	298	0.281	5,485,234	315.0	–15.0	0°	0.4

Differences of the VHPD analysis and ellipsoid model from the dipole model

Model	Statistic1	Statistic2	Statistic3	Statistic4	% Data misfit
VHDP_50	7°	13	4	364	4
VHDP_200	3.4°	6	2	41	3
ellipsoid_50	2.2°	16	36	1,267	16
ellipsoid_200	1°	8	12	96	5

The dipole and ellipsoid models (but not the virtual VHPD models) map apparent spatial distributions of magnetisation from which distances between magnetisation and the magnetic field measurements can be estimated. However, for an unknown intensity of magnetisation a dipole model only constrains the shallowest magnetisation to be no deeper than its centre, and ellipsoid models also provide uncertain estimates of the elevation of the top of magnetisation. None of the model-misfit statistics S1 to S4 specify elevation of the top of magnetisation. They therefore do not directly report the separation distances between magnetisation and magnetic field measurements and/or computations; nevertheless, in combination with the statistics 1 to 4 as derived above they indirectly indicate the more general concept of proximity to magnetisation.

4.11 VHPD AND DE MAGNETIC FIELD ANALYSIS CASE STUDY NEAR KEMENDOK PARK, SOUTH-WEST NEW SOUTH WALES

Figure 4.17 shows the location of the study area close to the Kemendok National Park in south-west New South Wales, north of the Murray River and Victorian border. The local geomagnetic field has a declination of 10° and inclination −65°. The area is covered with a variable thickness of semi-consolidated, weakly magnetic Cenozoic Murray Basin sediments. The TMI image of the area shown in Fig. 4.18A is created from data acquired on the Murray Basin aeromagnetic survey flown in 2005 on east–west flightlines at a spacing of 400 m and nominal terrain clearance of 60 m. This data (survey P1105) is available for download from Geoscience Australia's Geophysical Archive Data Download (GADDS). The two anomalies analysed here can also be downloaded from The Australian Remanent Anomalies Database (ARAD numbers 355 and 356). Studies of their magnetisation directions are reported by Foss *et al.* (2024). Anomaly ARAD356 (Fig. 4.18A) has similar peak (+38 nT) and trough (−27 nT) amplitudes and a south-east directed trough to peak azimuth. In the steep southern hemisphere background field the similar peak and trough amplitudes suggest the resultant magnetisation has low inclination, and the trough to peak orientation suggests that the declination of magnetisation is to the south-east (c. 135°). Anomaly ARAD355 (Fig. 4.18A) in the south-east also has similar peak (+76 nT) and trough (−66 nT)

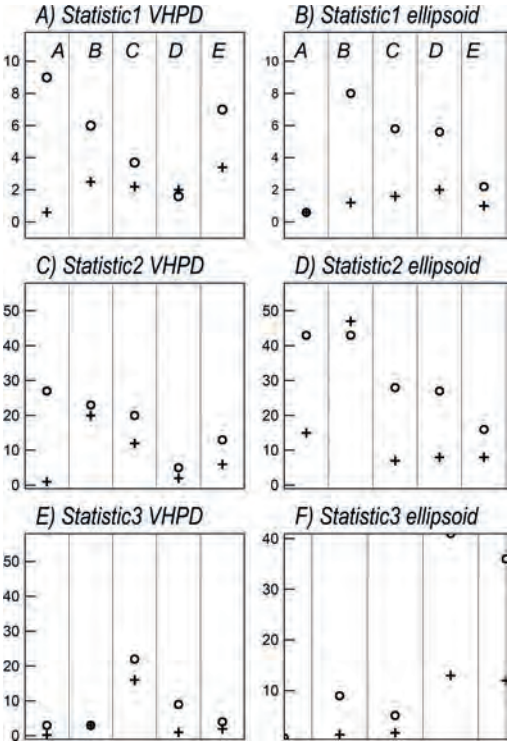

Fig. 4.15. Top to bottom S1 to S3 values, (left) VHPD analysis and (right) DE analysis. In each plot: column A is for equidimensional models, column B for models with magnetisation parallel to horizontal elongation, column C for models with magnetisation perpendicular to horizontal elongation, column D for models with magnetisation parallel to plunge azimuth and column E for models with magnetisation perpendicular to plunge azimuth. Circles are for 50 m elevation (more proximal fields) and crosses for 200 m elevation (more distal) fields.

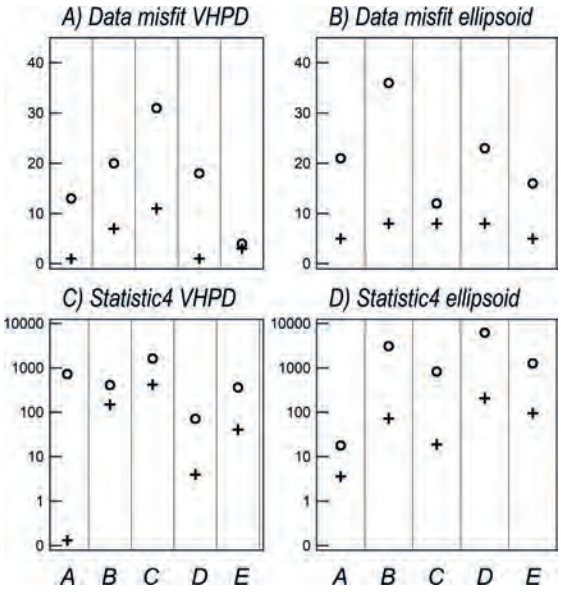

Fig. 4.16. Top row: data misfit and Bottom row: S4 values for (left) VHPD analysis and (right) DE analysis. Columns A to E and symbols are as in Fig. 4.15.

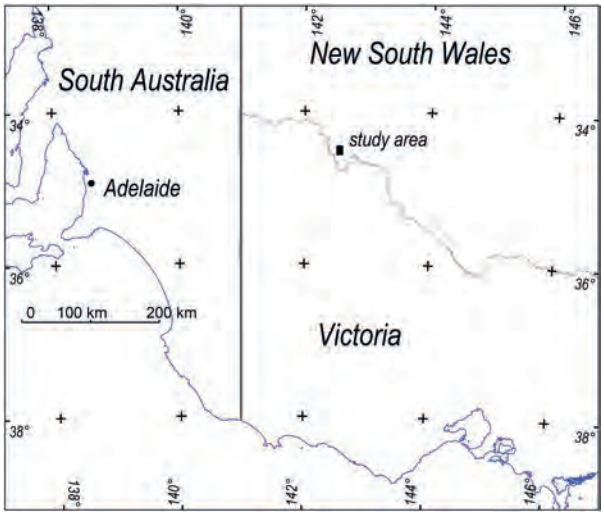

Fig. 4.17. Kemendok study area in south-west New South Wales.

amplitudes, in this case with south-south-west trough to peak azimuth, suggesting a low inclination south-south-west directed magnetisation. In the western half of the area are two less distinct, lower amplitude and almost completely negative anomalies (not investigated in this study) apparently due to steep positive inclination (reverse) magnetisations but these smaller, single-polarity anomalies are insufficiently sampled by the 400 m spaced flightlines for reliable magnetisation analysis.

The best estimates of source magnetisation for the two selected anomalies are derived from individual inversions to simultaneously find both the spatial distribution of magnetisation and its direction. Acceptable starting estimates of magnetisation direction are provided by the simple rules described above and the long-wavelength, low-amplitude regional field variations support reliable separation of the anomalous (residual) magnetic fields. Figures 4.19A and 4.19B show the close fits of measured and model-computed fields achieved using elliptic-section pipe models with horizontal top and base and with homogeneous magnetisation for the north-east and south-east anomalies respectively. Success of the models in matching the field does not prove them correct or that the magnetisations are homogeneous. The models should not be considered direct representations of the in-ground magnetisations but rather summary statistics of the magnetic moments and distributions of magnetisation. The horizontal-top faces of the models are interpreted as due to termination of the magnetisation at a sub-horizontal unconformity and the limited depth extents suggest that the bodies may

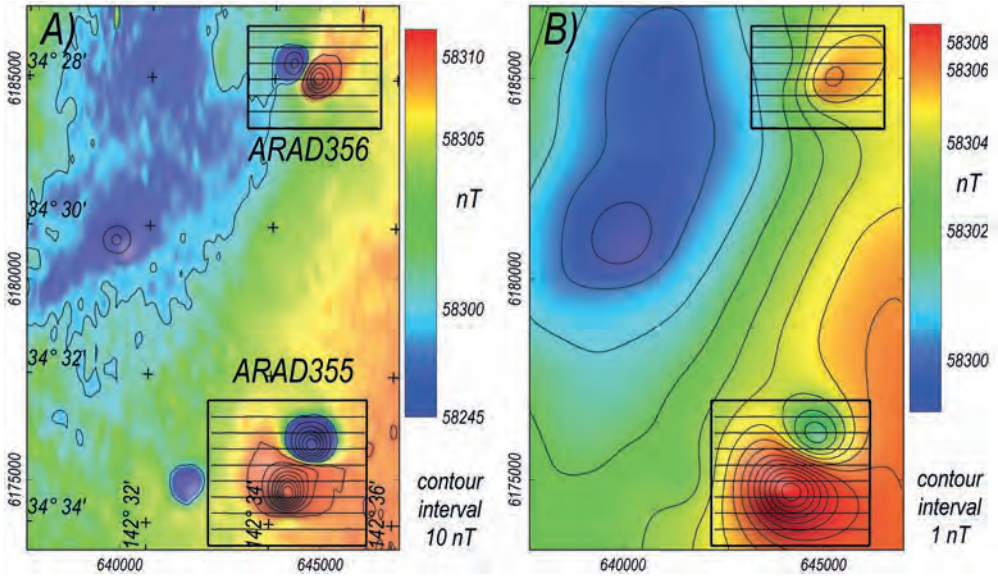

Fig. 4.18. TMI images of the Kemendok study area: A) measured TMI and B) upward continued by 800 m.

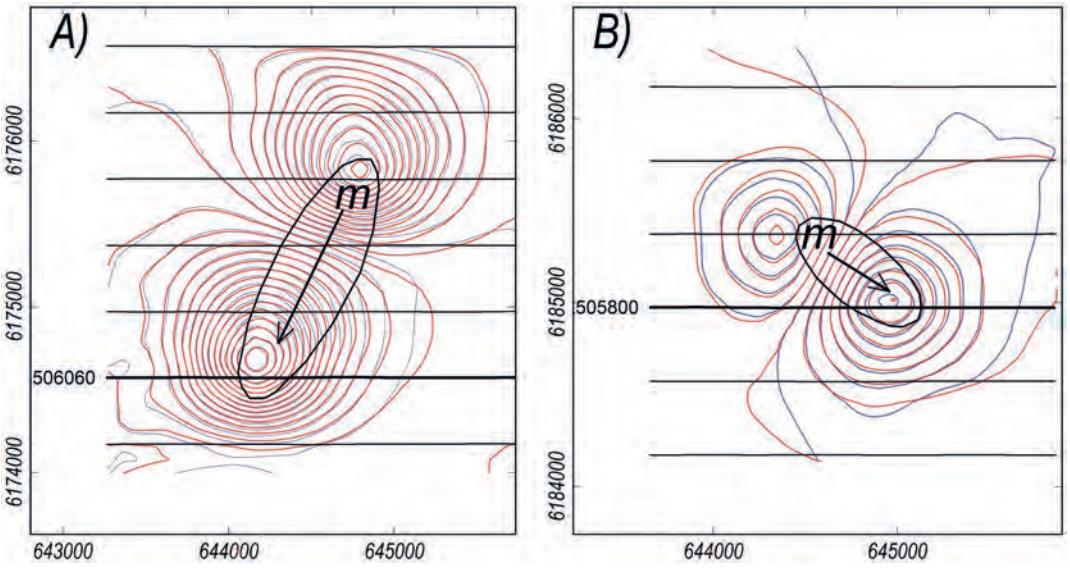

Fig. 4.19. TMI contours at 5 nT intervals measured (blue) and model-computed (red) of the best-fit elliptic-section pipes for anomaly ARAD355 (A) and ARAD356 (B) with orientation of the magnetisation vectors.

possibly be diatremes with only narrow undetected feeder zones rather than deep-going pipes. Declinations of resultant magnetisation derived by the inversions and plotted in Fig. 4.19 are parallel to elongation of the bodies. This most likely reveals a bias in estimating the shape of the anomalies arising from their magnetisation directions. Figure 4.20 shows contours of model-computed TMI fields from best-fit vertical circular pipe models. These models with fewer degrees of freedom do not match the measured anomalies as closely as the elliptic pipe models; however, the key statistics of the computed field peak and trough amplitudes and their locations are almost identical between the elliptic and circular pipe models and the model magnetisation directions only differ by 1° for anomaly ARAD356 and by 3° for anomaly ARAD356. The inversion results with the different geometry bodies illustrate that for these moderately proximal anomalies the direction of magnetisation is far more influential than the distribution of magnetisation in determining anomaly characteristics.

The distribution of magnetisation influences anomaly details but inversion does not have the power to reliably recover source information from those details. The only feasible (but unlikely) major deviation from these models would be to explain the anomalies as due to similar net low-inclination magnetisations consisting of separated steep positive and steep negative inclination magnetisations beneath the anomaly troughs and peaks respectively.

Figures 4.21A and 4.21B show sections along key west–east flightlines through the two anomalies. The best estimated depths to the top of magnetisation below the elevation of the magnetic field sensors are 215 and 195 m for anomalies ARAD355 and ARAD356 respectively. The diameters of the circular pipe models for the two anomalies are 1360 and 780 m, giving width to measurement separation ratios of 6 for anomaly ARAD355 and 4 for anomaly ARAD356, consistent with the anomalies being moderately proximal.

These proximal anomalies provide suitable tests of dipole inversions and VHPD and DE analyses. To contrast the analyses with those of a more distal field I upward continued the TMI grid by 800 m, interpolated the grid values onto the flight lines and inverted those channels, adding the 800 m upward continuation to the flying height as the elevation reference channel. The addition of 800 m to the estimated original sensor elevation of ~200 m above the top of magnetisation increased the virtual separation of the field measurements from the magnetisation by a factor of approximately 5,

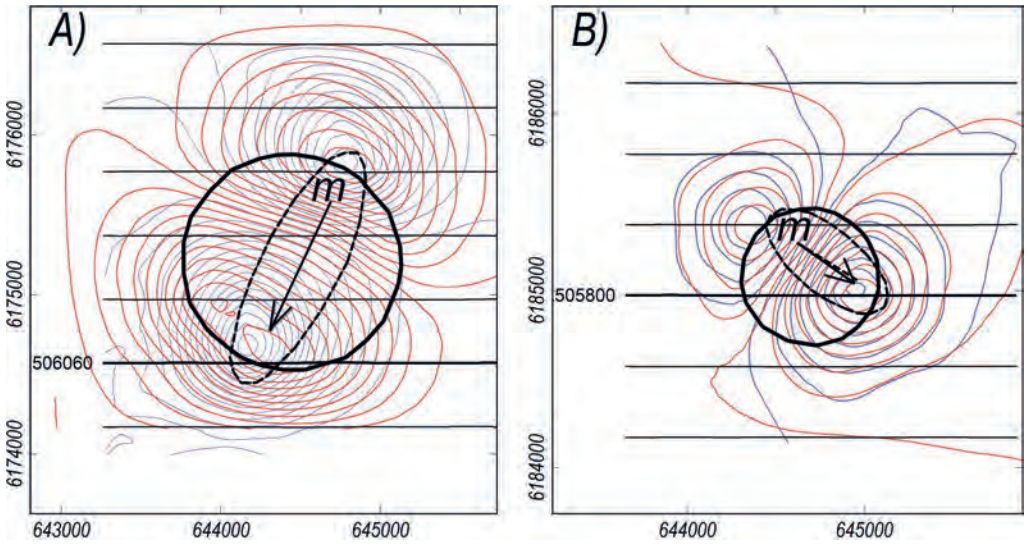

Fig. 4.20. TMI contours at 5 nT intervals measured (blue) and model-computed (red) of the best-fit vertical, circular-section pipes for anomaly ARAD355 (A) and ARAD356 (B) with orientation of magnetisation vectors. The elliptic pipe outlines are shown for comparison.

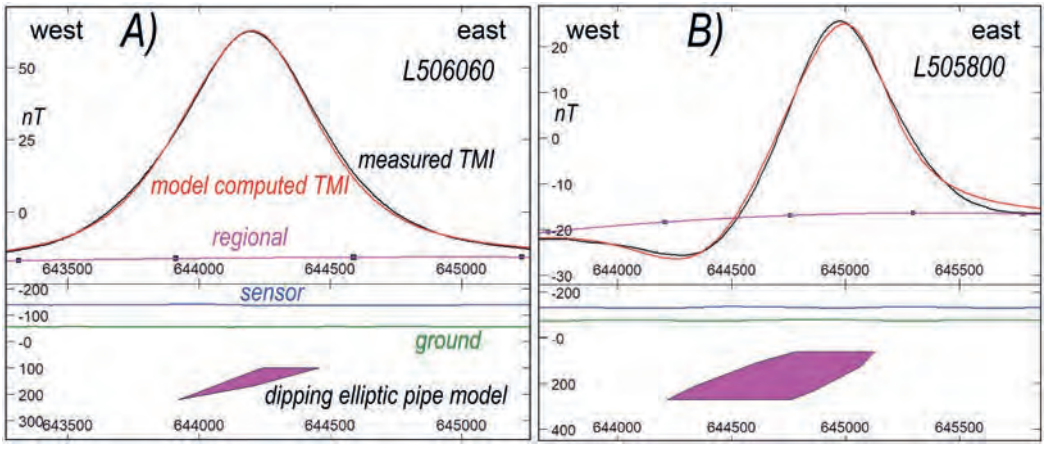

Fig. 4.21. Flightline model cross-section views for anomalies A) ARAD355 and B) ARAD356. The measured channel is in black, the background field in magneta and the model-computed field is in red.

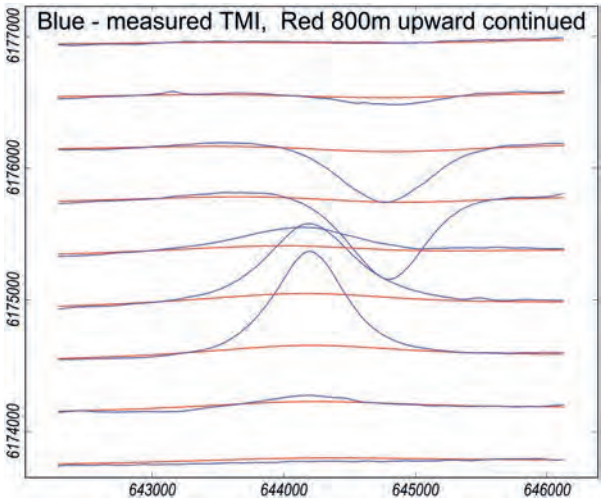

Fig. 4.22. TMI stacked profiles for Anomaly 355: measured (blue) and after 800 m upward continuation (red).

resulting in an anomaly width to magnetisation-field measurement separation ratio of ~1.2 for anomaly ARAD355 and ~0.8 for anomaly ARAD356. These values represent moderately distal fields with greatly reduced capacity to resolve detail of the distribution of magnetisation compared to the (already unreliable) resolution of spatial detail from the lower-level directly measured field. Attenuation of signal with the 800 m upward continuation is illustrated in Fig. 4.22 which shows stacked profiles of both the measured (blue) and upward continued (red) TMI channels. The attenuation is substantial and reliable modelling and inversion of the upward-continued data requires valid anomaly separation from the background field. This separation could not be performed reliably on the upward continued data because of the reduced contrast in curvature of the anomalous and background fields, and so the upward continuation was applied to a residual separation of the fields performed at the lower elevation.

I inverted the two anomalies using dipole and ellipsoid models. Figure 4.23A shows stacked profiles of measured TMI for anomaly ARAD355, together with stacked profiles of computed TMI from the best-fit dipole and ellipsoid inversion models. The computed field from the dipole model (the red curves) is clearly too simple to acceptably explain the measured field (the black curves), but nevertheless the estimated magnetisation direction is within 1° of the estimate from much closer data-fits of the ellipsoid model. The computed field from the ellipsoid model (the blue curves) still reveals minor unexplained detail in departure from the measured curves. The equivalent curves after 800 m upward continuation of the residual measured field (the measured field with the regional field from the modelling subtracted) are shown in Fig. 4.23B. At this elevation the dipole model provides a much closer fit to the measured field, and the curves for the measured field and the field computed from the ellipsoid model are almost identical, showing the greatly reduced sensitivity in distal fields to the distribution pattern of source magnetisation.

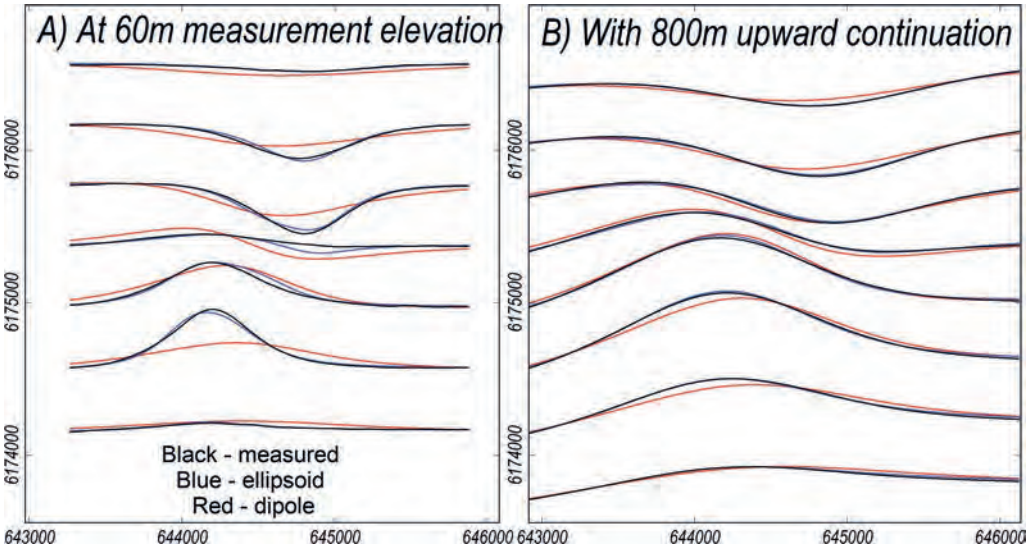

Fig. 4.23. TMI Stacked profiles for anomaly ARAD355: field data (black), computed from the elipsoid model (blue) and from the dipole model (red). A) at the initial measurement elevation of 60 m above ground and B) after an 800 m upward continuation.

Figure 4.24 shows in perspective view the best-fit elliptic pipe model for anomaly ARAD355 (in magenta), the best-fit dipole model (mesh in black), the best-fit ellipsoid model (dark green), and the vertical (red mesh) and horizontal (blue mesh) VHPD models. The dipole and VHPD model bodies are clearly poor representations of the distribution of magnetisation (that is best-estimated from the elliptic pipe model). The dipole model is centred close to the apparent centre of magnetisation but at significantly greater depth. The ellipsoid model (for which the computed field closely matches the measured field) is almost co-incident with the elliptic pipe model. Parameters of the various models and their analysis statistics are reported in Table 4.7 for field inversions of both the measured data and of the field after 800 m upward continuation. The percentage data misfits of the inversions at the two elevations do not change substantially. The estimated angular error of the VHPD inversion falls from 10° in the proximal field to 5° in the distal field, but the DE analysis increases from 0° to 4°. There are regular improvements in the VHPD and DE statistics from the proximal to distal inversion statistics, with significant reductions in the compound S4 statistic from 2640 to 45 for the VHPD analysis and from 226 to 35 for the DE analysis.

Figure 4.25 shows contours of measured field (black) and dipole model computed field (red) at the original survey height (Fig. 4.25A) and the 800 m upward continuation (Fig. 4.25B). The dipole model produces a reasonable fit to the measured field at the survey height and a closer fit in the more distal field at the upward continuation height. At the lower elevation the separation of the VHPD analysis dipoles of 900 m (Fig. 4.25A) is far less than the 1,300 m separation of the anomaly peak and trough. At the 800 m upward continuation height (Fig. 4.25B) the separation of the corresponding dipoles reduces to 88 m although the peak to trough separation increases to 1575 m. Figure 4.25 clearly shows the reduced influence of the distribution of magnetisation from the more proximal field (Fig. 4.25A) to the more distal field (Fig. 4.25B) and the influence of this in the location of the individual dipole virtual source analysis.

There are nearby anomalies from sources of similar size and at similar depth that appear to be due to steeply inclined magnetisations (although these anomalies might be influenced by poor sampling on the east–west flightlines). This introduces possible alternative models in which the preferred single body models are replaced with two bodies of opposite, steep magnetisation (much like the virtual VHPD models). Figure 4.26A and Fig. 4.26B show perspective models for anomalies ARAD355

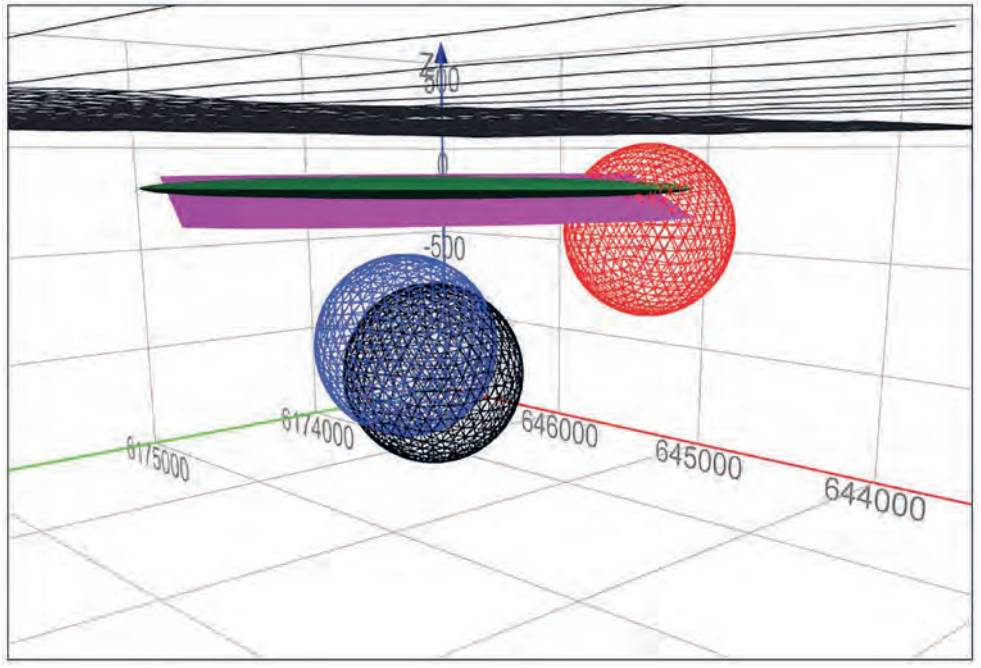

Fig. 4.24. Models for anomaly ARAD355: Elliptic-section pipe (magenta), ellipsoid (dark green), best dipole (black) and vertically polarised (blue) and horizontally polarised (red) combined sphere model.

Table 4.7. ARAD355 model and analyses statistics.
* rot_n is the angular rotation (in degrees) from the best-estimated magnetisation direction of the elliptic pipe inversion (undefined for the individual V and H dipoles).

Model	Top Xc	Top Yc	Z_{centre}	Depth to centre below sensor	J (A/m)	Vol (m^3)	Dec_n degrees	$Inc._n$ degrees	rot_n* degrees	Data misfit %
Best pipe (TMI)	644,636	6,175,170	–167	301	2.645	$6.11x10^7$	206	–2	–	7
Dipole	644,449	6,175,241	–747	884	3.516	$11.31x10^7$	206	–2	0°	10
Dip_V	644,129	6,174,519	–747	884	0.630	$11.31x10^7$	000	–90	–	–
Dip_H	644,466	6,175,274	–747	884	2.933	$11.31x10^7$	206	0	–	–
VHPD	644,410	6,175,136	–747	884	3.000	$11.31x10^7$	206	–12	10°	9
Ellipsoid	644,464	6,175,212	–139	886	3.252	$4.767x10^7$	206	–2	0°	4
Best pipe (UC800)	644,588	6,175,235	–73	1,010	0.579	$23.7x10^7$	207	–6	4°	6
Dipole	644,439	6,175,197	–403	1,340	1.606	$11.31x10^7$	207	–7	1°	12
Dip_V	644,528	6,175,194	–403	1,340	0.190	$11.31x10^7$	000	–90	–	–
Dip_H	644,440	6,175,196	–403	1,340	1.607	$11.31x10^7$	212	0	–	–
VHPD	644,449	6,175,196	–403	1,340	1.618	$11.31x10^7$	212	–7	5°	12
Ellipsoid	644,438	6,175,217	–100	1,037	0.771	$18.05x10^7$	207	–6	4°	5

Model	Statistic1	Statistic2	Statistic3	Statistic 4 (Product S1.S2.S3)	% Data misfit
VHDP 50	10°	22	12	2,640	9
VHDP 800	5°	9	1	45	12
Ellipsoid 50	1°	61	3.7	226	4
Ellipsoid 800	1°	23	1.5	35	5

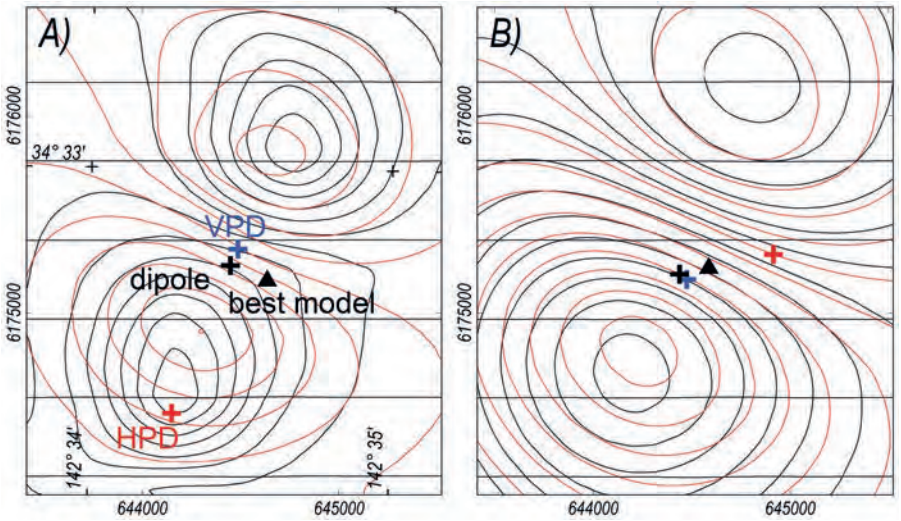

Fig. 4.25. TMI contours for anomaly ARAD355: measured field (black) and best-dipole computed field (red), A) at meaurement elevation of 60 m above ground and B) after 800 m upward continuation. Centres of the best pipe (black triangle), best dipole (black cross) and vertically polarised (red cross) and horizontally polarised (blue cross) dipole pair model are also plotted.

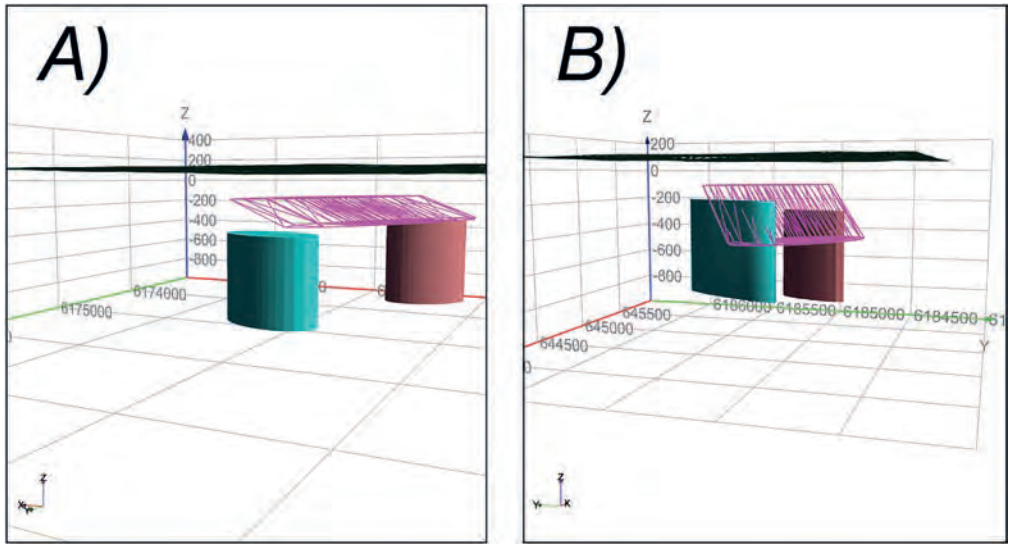

Fig. 4.26. Elliptic pipe (magenta) and dual-polarity vertical elliptic pipe (blue negative inclination and brown positive inclination) models for anomalies A) ARAD355 and B) ARAD356.

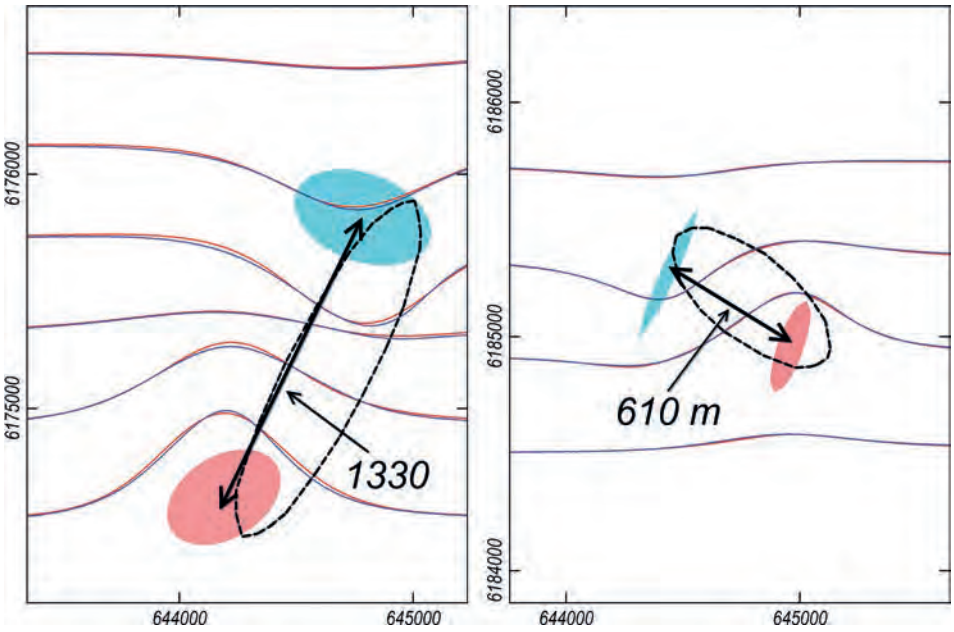

Fig. 4.27. Stacked profiles of fields computed from the best-fit elliptic pipe model (blue) and dual-polarity vertical elliptic pipe (blue negative inclination and brown positive inclination) models (red) for anomalies A) ARAD355 and B) ARAD3561.

and ARAD356 respectively, using two vertical pipes of steeply inclined opposite polarity magnetisation. These pipes are approximately centred beneath the anomaly peaks and troughs, and as shown in Fig. 4.27 are close to the ends of elliptic pipe models that are elongated (apparently artificially) in the magnetisation directions. Figure 4.27 shows stacked profiles of the field computed from the elliptic pipe models (that I believe to be the best representative models of the magnetisations) and of the field computed from the dual vertical pipe bodies of opposite-polarity, steep-inclination magnetisation. The stacked profiles match closely, with slightly greater misfit for the more elongate anomaly ARAD355 (Fig. 4.27A) for which the measured field is effectively more proximal than for the more compact anomaly ARAD356 (Fig. 4.27B).

Fields computed after switching the positions of the bodies in the dual-pipe models (and thereby switching

the peak and trough of that computed field) produces fields that can be closely matched using the original single elliptic pipe model with a rotation of 180° in its declination of magnetisation. This clearly demonstrates the role that the distribution of magnetisation plays in these models of extreme inhomogeneity of two magnetisations of very different direction. The ambiguity of possible multiple magnetisations extends to distal fields.

4.12 CONCLUSIONS

The concept of proximal and distal fields relates specifically to the information carried in a magnetic field about its source magnetisations and plays a critical role in evaluation of what information can be reliably recovered from magnetic field analysis. The ultimate distal field is of a dipole source that is completely specified by its centre coordinates and total magnetisation (including direction). Circular or elliptic anomalies in a magnetic field dataset can in the first instance be matched with a dipole model and if that is found insufficient then additional complexity can be progressively introduced as justified.

I propose vertically and horizontally polarised dipole (VHPD) analysis as a means to measure coherent departure of a measured magnetic field from that due to a dipole. The statistics of VHPD analysis can be incorporated with statistics derived from best-fit dipole and best-fit ellipsoid models as an aid to evaluate the degree of additional detail that is justified in a magnetisation model.

In this study I first used a synthetic model of a complex equidimensional magnetisation to show that a dipole model can reasonably recover both the horizontal centre of magnetisation and the direction of that magnetisation. The magnetic field expression of shape details reduces at higher elevations as the match with the best-fit dipolar model field improves. I then used dipoles, polarised dipoles and ellipsoids to invert magnetic fields of horizontally elongated magnetisations. It is difficult to estimate magnetisation directions of horizontally elongate bodies that can alternatively be represented as polarisations towards their ends, and additional challenges in recovering magnetisation direction are encountered in analysis of plunging magnetisations. At low elevations magnetisation at the shallowest end of a plunging elongate source dominates the magnetic field and may distort estimation of magnetisation direction. At higher elevations the magnetic field has a weaker bias to the influence of plunge and estimates of both the centre of magnetisation and of magnetisation direction are more dependable.

I have presented a case study of inversion and VHPD analysis of two magnetic anomalies measured in southwest New South Wales over what are believed to be volcanic bodies intruded above or into basement beneath a cover of younger sediments. The anomaly patterns reveal that the anomalies are predominantly due to remanent magnetisations differently directed to the local geomagnetic field. I inverted each anomaly independently, in both cases making an interpretive separation of the anomalous field due to the magnetisations from what I believe to be the background field. The best estimate of source magnetisation direction for the sources of these anomalies is derived from inversion using elliptic-section pipes with horizontal top and bottom surfaces. Alternative inversions using ellipsoid bodies produces models with similar spatial distribution and almost identical resultant magnetisation direction, but these bodies are less useful for estimation of depth to the top of magnetisation. Inversion using dipole models provided similar estimates of the centres and directions of magnetisation but coherent departures in matching the measured field reveal that the magnetisations are insufficiently represented by homogeneous spherical magnetisations and that the fields are therefore to some degree proximal. VHPD and DE analysis of these field anomalies applied to the original survey data and to more distal data derived from an 800 m upward continuation match the characteristics predicted from the synthetic modelling studies.

REFERENCES

Clark DA, Saul SJ, Emerson DW (1986) 'Magnetic and gravity anomalies of a triaxial ellipsoid'. *Exploration Geophysics* **17**, 189–200. doi:10.1071/EG986189

Foss CA, Hope JA, Patabendigerada S (2024) 'Regional magnetic depth estimates for the Eastern Resources Corridor (ERC), Officer Basin, Tasmania, and Northeast Queensland'. eCat No. 149239.

Hood PJ (1964) 'The Königsberger ratio and the dipping dyke equation'. *Geophysical Prospecting* **12**, 440–456. doi:10.1111/j.1365-2478.1964.tb01916.x

This page intentionally left blank